

Can the Gulf Stream induce coherent short-term fluctuations in sea level along the US East Coast? A modeling study

Tal Ezer¹

Received: 24 August 2015 / Accepted: 25 January 2016 / Published online: 4 February 2016
© Springer-Verlag Berlin Heidelberg 2016

Abstract Much attention has been given in recent years to observations and models that show that variations in the transport of the Atlantic Meridional Overturning Circulation (AMOC) and in the Gulf Stream (GS) can contribute to inter-annual, decadal, and multi-decadal variations in coastal sea level (CSL) along the US East Coast. However, less is known about the impact of short-term (time scales of days to weeks) fluctuations in the GS and their impact on CSL anomalies. Some observations suggest that these anomalies can cause unpredictable minor tidal flooding in low-lying areas when the GS suddenly weakens. Can these short-term CSL variations be attributed to changes in the transport of the GS? An idealized numerical model of the GS has been set up to test this proposition. The regional model uses a $1/12^\circ$ grid with a simplified coastline to eliminate impacts from estuaries and small-scale coastal features and thus isolate the GS impact. The GS in the model is driven by inflows/outflows, representing the Florida Current (FC), the Slope Current (SC), and the Sargasso Sea (SS) flows. Forcing the model with an oscillatory FC transport with a period of 2, 5, and 10 days produced coherent CSL variations from Florida to the Gulf of Maine with similar periods. However, when imposing

variations in the transports of the SC or the SS, they induce CSL variations only north of Cape Hatteras. The suggested mechanism is that variations in GS transport produce variations in sea level gradient across the entire GS length and this large-scale signal is then transmitted into the shelf by the generation of coastal-trapped waves (CTW). In this idealized model, the CSL variations induced by variations of ~ 10 Sv in the transport of the GS are found to resemble CSL variations induced by $\sim 5 \text{ m s}^{-1}$ zonal wind fluctuations, though the mechanisms of wind-driven and GS-driven sea level are quite different. Better understanding of the relation between variations in offshore currents and CSL will help to improve the prediction of both short-term water level anomalies that cause flooding, as well as spatial variations in long-term sea level variability and coastal sea level rise.

Keywords Gulf Stream · Florida Current · Sea level · Climate change · Numerical model · Coastal waves

1 Introduction

The proposition that variations in the intensity of the Gulf Stream (GS) current can cause coastal sea level (CSL) variations along the US East Coast has been suggested early on (Montgomery 1938) and even verified to some degree by limited early observations (Blaha 1984). A simple wind-driven Rossby wave model (Sturges and Hong 2001) and early three-dimensional ocean circulation models (Ezer 1999, 2001) found that decadal variations in the circulation of the North Atlantic Ocean and in the Gulf Stream in particular are correlated with CSL variations along the western boundary of the North Atlantic. In general, a weakening in the GS transport reduces the sea level gradient across the current (assumed to be near a geostrophic balance) and thus

Responsible Editor: Leo Oey

This article is part of the Topical Collection on the *7th International Workshop on Modeling the Ocean (IWMO) in Canberra, Australia 1–5 June 2015*

✉ Tal Ezer
tezer@odu.edu

¹ Center for Coastal Physical Oceanography, Old Dominion University, 4111 Monarch Way, Norfolk, VA 23508, USA

increase/decrease sea level in the onshore/offshore side of the GS; changes in the GS transport can thus be detected through the difference in sea level between Bermuda and the US East coast, as found by previous studies (Ezer 1999, 2001, 2015; Sturges and Hong 2001). As a result, a weakening in the GS is often associated with increased flooding on long stretches of the western boundary of the North Atlantic (Sweet et al. 2009; Ezer and Atkinson 2014; Sweet and Park 2014; Goddard et al. 2015). However, the exact mechanism that can be responsible for transmitting an offshore signal onto the shelf and creating coherent CSL anomalies along thousands of kilometers of coastlines is not fully understood. Process studies (Huthnance 2004) and satellite observations (Hughes and Meredith 2006) suggest that large-scale oceanic motions are transmitted to the shelf through the generation of coastal-trapped waves (CTW); the result is often coherent CSL signals along large stretches of coastlines. CTW cover a wide range of time and length scales and different types of waves, such as barotropic and baroclinic Kelvin waves, topographic Rossby waves, and continental shelf waves (Allen 1975; Wang and Mooers 1976; Huthnance 1978). The transmission of the offshore signal to the shelf depends on several parameters such as the slope and shelf topography, stratification, friction, as well as the frequency and length scales of the forcing. Huthnance (2004) indicated that coastal tide gauges can be especially effective monitors for the largest-scale oceanic signals. Zhao and Johns (2014) shows that wind-driven variations over the sub-tropical gyre can result in coherent variations along the GS path over thousands of kilometers, so that the open ocean-shelf transmitting mechanism discussed by Huthnance seems possible for those GS signals. There are also some differences in the CTW's characteristics between waves with periods shorter or longer than ~10 days, whereas in the higher frequency range, near-resonance CTW can amplify the coastal response (Huthnance 2004). Model results, discussed later, focused on oscillations with periods of up to ~10 days—they will be evaluated to see if CTW may have been generated by variations in the GS transport.

The GS itself is the upper branch of the Atlantic Meridional Overturning Circulation (AMOC) which is affected by the North Atlantic Oscillations (NAO) and other climatic changes. The connection between ocean circulation and CSL can be seen in various observations, such as satellite altimetry (Ezer et al. 2013), the cable measurements of the Florida Current (FC; Baringer and Larsen 2001; Ezer 2013), or the recent AMOC observations (McCarthy et al. 2012; Ezer 2015). On time scales even longer than interannual and decadal, data suggest that multi-decadal variations and recent acceleration in sea level rise (SLR) along the US East Coast (Boon 2012; Ezer and Corlett 2012; Sallenger et al. 2012; Kopp 2013; Ezer 2013; Ezer et al. 2013), may reflect a dynamic response to climatic changes in ocean circulation (Levermann et al. 2005; Yin and Goddard 2013) and slowing down of AMOC

(Smeed et al. 2013; Bryden et al. 2005; Ezer 2015; Srokosz and Bryden 2015). There is also a very distinct spatial pattern in variations of sea level along the coast (e.g., see Fig. 3 in Ezer 2013), that may relate to the GS dynamics. In the region from Florida to Cape Hatteras (the South Atlantic Bight, SAB) the GS flows northward relatively close to the coast, while in the region north of Cape Hatteras (the Mid-Atlantic Bight, MAB, and farther north) after the GS has separated from the coast, one finds the Northern Recirculation Gyre (Mellor et al. 1982; Hogg 1992) which separates between the GS and the coast; this gyre is fed up by the cold Slope Current (SC; Rossby et al. 2010, 2014) coming from the north. The combined effect of this gyre, meso-scale activities of the GS meandering and eddies and the influence of large estuaries (e.g., Chesapeake and Delaware Bays) make the impact of the GS on the MAB coast more complex than farther south. In addition, recent studies call the MAB region a “hotspot for accelerated sea level” (Sallenger et al. 2012) and a “hotspot for accelerated flooding” (Ezer and Atkinson 2014), with a distinct dynamics that is different than that of the SAB, as can be seen in sea level data (Sallenger et al. 2012; Ezer 2013; Boon and Mitchell 2015) and models (Yin and Goddard 2013).

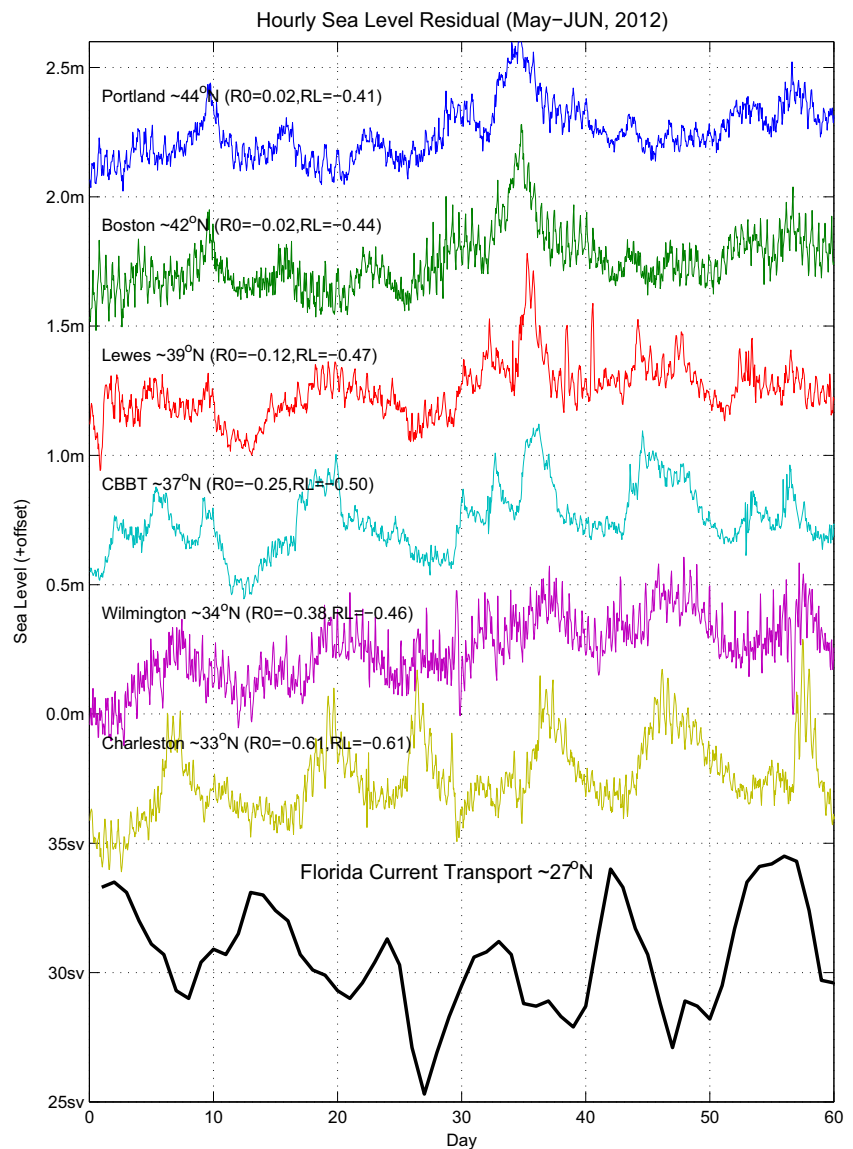
The fact that the GS impacts CSL is commonly attributed to the sea level gradient (~1–1.5-m height difference over ~100-km distance) across the GS whereas sea level is lower/higher on the onshore/offshore side of the GS in accordance with the geostrophic balance, so changes in the path and strength of the GS are expected to impact CSL variations; the mechanism of open ocean-coastal coupling is not so clear yet, and may involve CTW, as discussed before. The motivation for this study is twofold: First, the exact mechanism of the GS-driven CSL has not been completely explained or separated from other drivers of CSL. For example, coherent variations of CSL variations along the coast can also result from wind-driven sea level (Woodworth et al. 2014; Zhao and Johns 2014) vertical divergence of large-scale ocean currents (Thompson and Mitchum 2014), from the impact of atmospheric pressure (Piecuch and Ponte 2015) or changes in the southward flowing Slope Current (Rossby et al. 2010); changes in the latter may relate to climatic change in sub-polar regions (Hakkinen and Rhines 2004) or in the flow of coastal Labrador waters into the region (Xu and Oey 2011). Second, even if the GS contributes to variations in CSL, it is not clear on what time scales this driver may be valid. As indicated in the summary earlier, much of the attention in recent years was given to CSL variations on long time scales ranging from interannual to decadal and multi-decadal. However, there is evidence (see Fig. 9 in Ezer and Atkinson 2014) that even on short time scales of days and weeks weakening of the GS, as measured by the transport of the FC in the Florida Straits, is reflected in anomalously high water levels and an unpredictable tidal flooding. These anomalies cannot be easily explained by any of the mechanisms mentioned

earlier. Intriguingly enough, Ezer and Atkinson (2014) show almost no lag between the time of detection of significant changes in the flow through the Florida Straits and high water anomalies observed thousand kilometers farther downstream on the Mid-Atlantic coasts, suggesting large-scale forcing and fast propagation of signals.

Figure 1 is an example of hourly CSL variations during a 2-month period (May–June, 2012) at 6 tide gauge stations (see Fig. 2a for locations) and the daily FC transport at the same time. There is no particular reason for choosing this period, but it is very typical to almost any other time when there are no major storms. The shown CSL is the residual after tides have been removed (by tide prediction models for each station); the residual is often referred to as the sub-tidal wind-driven part of the CSL signal, though it can include other influences. The CSL shows variations on scales ranging from a few hours to apparent oscillations with periods between 2 and 10 days

(typical scale for wind- and pressure-driven weather events). The FC transport (bottom of Fig. 1) shows mostly oscillations with range of up to ~10 Sv (1 Sverdrup = $10^6 \text{ m}^3 \text{ s}^{-1}$) and period of ~10 days (which may also be affected by weather events). Since the FC data is based on daily averages, higher frequency oscillations are likely suppressed. There are clear coherent variations in CSL over ~2000 km of coastline, see for example the high peaks in days 35–37 (though the southernmost point lags behind the northernmost point by ~2 days). However, there are periods (days 0–10 and 40–50) in which there are coherent variations in the SAB that are out of phase with variations in the MAB and north; Cape Hatteras (at ~36° N) seems to separate between these two regimes. The largest anti-correlation ($R = -0.61$) between the FC at 27° N and CSL farther north is at Charleston (statistically significance at 95 % confidence level), which is more than 600 km north of the Florida Straits. The significance of the correlation is reduced

Fig. 1 Examples of hourly sea level (colored lines; vertically shifted for clarity) at 6 tide gauge stations (see location in Fig. 2a) and the daily Florida Current transport (black heavy line) for May–June 2012. The correlation between daily averaged sea levels and the daily FC transport are indicated in parenthesis (the correlation coefficient R_0 is for zero lag and RL is the maximum correlation with lag of up to 8 days)



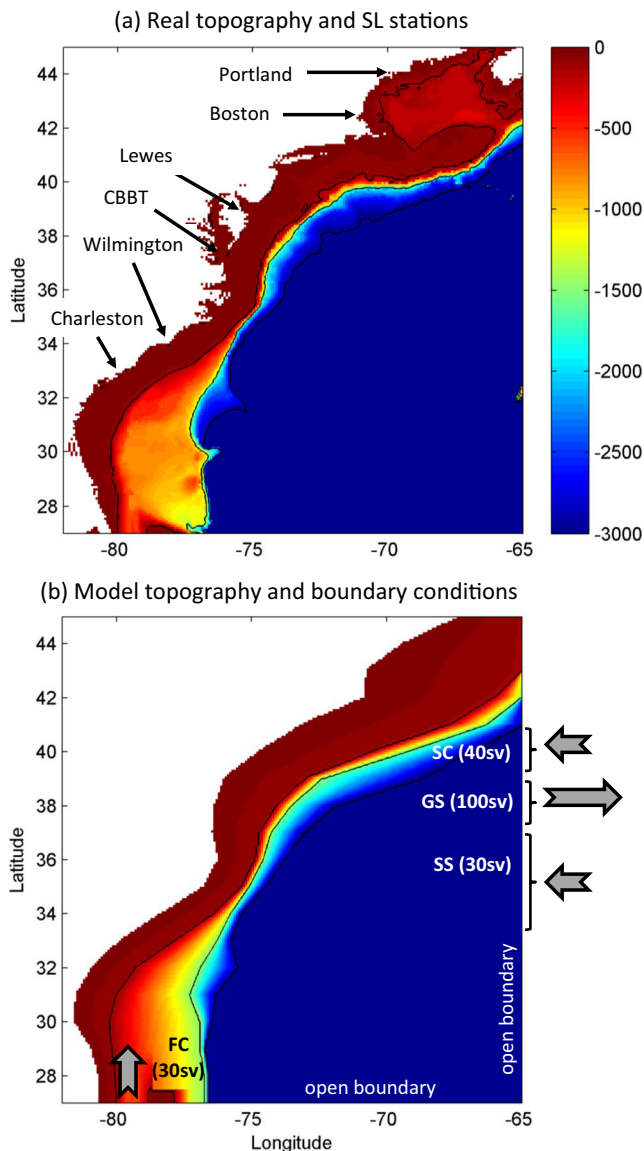


Fig. 2 **a** The bottom topography (depth in m) of the study area from ETOPO5 data and location of tide gauge stations. **b** The simplified topography of the numerical model and the boundary conditions in the control run (transport in $Sv = 10^6 \text{ m}^3 \text{ s}^{-1}$); inflows include the Florida Current (FC), the Slope Current (SC) and the Sargasso Sea (SS), and the outflow is the Gulf Stream (GS)

with the distance between the FC and the tide gauges because of phase lags, but if lags of a few days are allowed, persistent correlations of -0.4 to -0.6 are found along the entire coast. The negative correlation is consistent with the hypothesis highlighted earlier that a weakening geostrophic flow is related to lesser sea level gradients across the GS and increased CSL; CTW may then distribute the signal on the shelf. It is estimated from the square of the correlations that ~ 20 – 40 % of the CSL variability can be attributed to variations in the FC (though one must keep in mind that correlation does not mean causation, unless a plausible mechanism for such relation is shown). The observations in Fig. 1 are only meant to

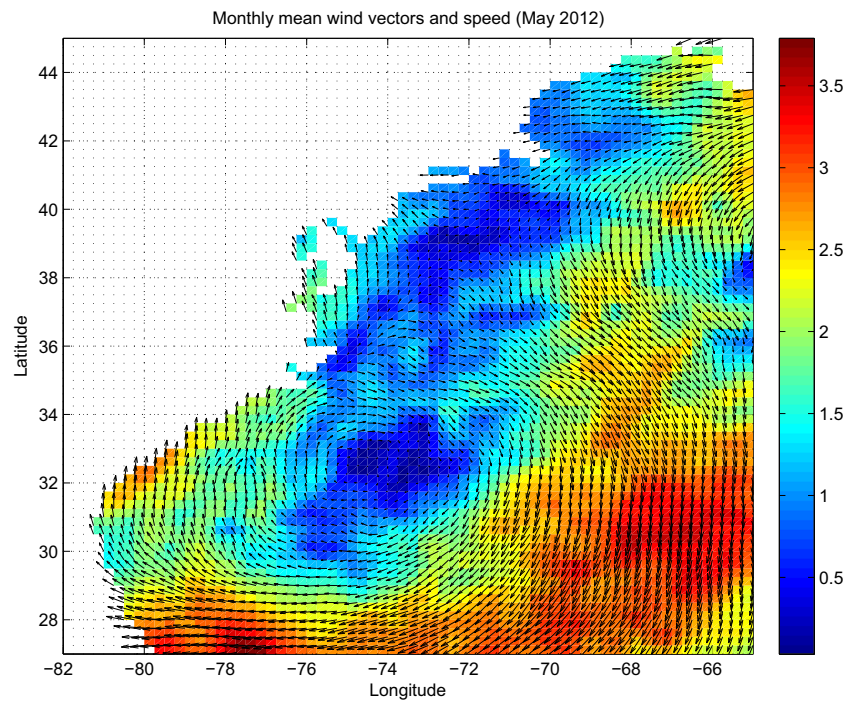
demonstrate the coherency of the short-term CSL variability and motivate the modeling study to better understand basic processes; a study to explain all the details of the observed data will need much longer sea level records and is beyond the scope of this study.

Therefore, in this study, a regional numerical ocean circulation model has been set up to test if short-term variations in the GS can really induce variations in CSL. The idealized model configuration (Fig. 2b) is not aimed at creating as realistic as possible simulations, but rather aimed at separating the GS impact from other forces, and perform sensitivity experiments that are not possible in the real ocean. The paper is organized as follows. First, the model setup and the experiments are described in section 2, then the results from different simulations are analyzed in section 3, and finally, discussions and conclusions are offered in section 4.

2 Numerical model setup

The model is based on the generalized coordinate numerical ocean circulation model of Mellor et al. (2002) with a terrain-following vertical grid, a Mellor-Yamada turbulence scheme and Smagorinsky-type horizontal diffusion (this model evolved from the Princeton Ocean Model; see Mellor et al., for details). Using this model with an idealized topography and forcing (e.g., as in Ezer 2006) is a useful way to study various processes in a more controlled environment than in realistic, more complex models. Therefore, the model topography uses a smoothed coastline (Fig. 2b) that resembles the real coastline (obtained from the ETOPO5 data, Fig. 2a), but eliminates the impact from rivers, estuaries, barrier islands, etc. The minimum depth is set to 10 m and the maximum depth is set to 3000 m; the main focus of the research is on the upper ocean so eliminating the very deep ocean has no impact on the results, while allowing a longer time step (barotropic and baroclinic time steps of 17 s and 8 min, respectively, were used). The model is driven at the surface by a constant monthly mean wind (May 2012, as in Fig. 1), shown in Fig. 3; wind data were obtained from advanced scatterometer (ASCAT) (Bentamy and Fillon 2012). Surface heat and freshwater fluxes are set to zero. Though Ezer and Mellor (1992) show the importance of heat flux for getting a realistic GS separation in long-term simulations, they can be neglected for the very short-term idealized simulations conducted here. Inflow/outflow transports are imposed on the eastern and southern open boundaries as vertically averaged velocities at fixed locations (Fig. 2b shows those transports for the control run). Internal velocities at each level are dynamically adjusted by the model's baroclinic equations given the density field near the boundary. The horizontal grid is a Cartesian grid with 1/12 resolution (~ 6 – 8 -km grid size) and the vertical depth-scaled grid has 21 layers with higher

Fig. 3 Monthly mean wind (color is speed in m s^{-1}) for May 2012



resolution near the surface (e.g., the thickness of each layer vary from $\sim 1/1000$ th to $1/15$ th of the water depth between the surface and bottom layers). Note that the model domain and its boundary inflow/outflow conditions are very similar to the early regional GS models of Mellor and Ezer (1991) and Ezer and Mellor (1992); the main changes from the previous to the current model is the higher resolution, smoother coastline, and the focus on short-term variability. The recirculation gyres north and south of the GS are important parts of the GS dynamics, as seen in observations (Hogg 1992) and in diagnostic calculations of the Atlantic Ocean circulation (Mellor et al. 1982; Ezer and Mellor 1994; Ezer et al. 1995). Therefore, regional models must include these gyres in their boundary conditions to obtain a realistic GS, as demonstrated by the GS separation experiments of Ezer and Mellor (1992). Here, three inflow transports are imposed: the Florida Current (FC), the Slope Current (SC), and the Sargasso Sea (SS) and their total transport is equal to the outflow of the Gulf Stream (GS), as seen in Fig. 2b. The location of the FC inflow on the southern boundary (27°N) is at 79°W – 79.75°W and the location of the GS outflow on the eastern boundary (65°W) is at 37°N – 39°N (with the SC and SS inflows located north and south of the GS, respectively, as seen in Fig. 2b). The fixed location of the GS outflow (and all other inflows on the eastern boundary) may damp some variations in the eastern side of the domain, but adding a variable GS location will add another parameter that will make assessment of the impact of transport variations more difficult. Only the total transport (vertically integrated velocity) is specified on the boundary together with standard barotropic radiation boundary

conditions to minimize artificial reflection of waves from the boundary. The vertical distribution of the velocity near the open boundaries is calculated by the model from the density field in a 1° buffer zone near the southern and eastern open boundaries. Note that the open boundary conditions do not guarantee an exact conservation of the volume within the model domain; however, variations in the area averaged surface elevations seem very small ($\sim 1 \text{ cm}$), so the radiation conditions do not seem to pose any problem or climate drift, at least for the short simulations analyzed here.

Initial condition is the monthly mean temperature and salinity field obtained from reanalysis data (Ferry et al. 2012) for May 2012. The data are interpolated from the $1/4^\circ$ grid and 33 vertical layers into the model grid. Since the main interest is in idealized short-term simulations (hours to weeks) the timing of the start of the simulations is not critical, as long as a quasi realistic-looking GS is obtained. Note however, that for long-term simulations, one may need to add time-varying winds, freshwater, surface heat fluxes, etc., as has been done in more realistic models of the region that are used for process studies (Xu and Oey 2011) or operational forecast systems (Aikman et al 1996); this kind of realistic simulation is beyond the scope of this study. Because of the small domain, the constant forcing, and the strong influence of the imposed boundary conditions, the three-dimensional velocity field and the surface elevation in the model are dynamically adjusted to the density field very quickly, so after 10 days of diagnostic calculations (holding temperature and salinity unchanged) and another 20 days of prognostic calculations, a near steady-state is reached as shown in previous diagnostic-prognostic

calculations (Ezer and Mellor 1994; Ezer et al. 1995). During the last 10 days of this spin-up, mean and eddy kinetic energy reach almost a constant value except natural fluctuations due to the meandering GS. All experiments start from this dynamically adjusted field after spin-up, and produce quite realistic GS simulations as seen from instantaneous images of sea surface height (SSH) and sea surface temperature (SST) (Fig. 4). One can see for example the generation of two cold-core eddies (around 35° N) and one warm-core eddy (around 39° N); all eddies propagate westward as expected. Also notice that the CSL in the MAB north of Cape Hatteras is lower (darker blue in Fig. 4a, b) than the CSL along the SAB coasts in the south. For many years, this downward tilt in sea level as one moves north along the coast has been a topic of controversy and disagreement between geodesists and oceanographers (Sturges 1974). While the direction of the along-shore tilt (downward northward) in our relatively simple model generally agrees with the results from observations and other models (Higginson et al. 2015), there are some differences. For example, our model shows a larger jump in shelf sea level at Cape Hatteras than shown in Higginson et al.'s results. Note also, that river and coastal Labrador water flows may tend to create in the MAB a CSL tilt in opposite direction to that induces by the GS (Xu and Oey 2011). In any case, the current study is not intended for studying the details of the along-coast sea level tilt, which will require more realistic topography and forcing and longer simulations to capture possible seasonal variations in the sea level over the shelf.

Seven different simulations are conducted in order to see the sensitivity of the CSL in the model to fluctuations in

inflows and wind; Table 1 summarized the experiments. Note again, that the experiments are not meant to simulate realistic conditions as observed in Fig. 1, but to be able to isolate different processes under idealized and controlled conditions. All simulations are for 60 days following the spin-up, saving output fields at 6-h intervals, but neglecting the first 5 days which are a little noisier—otherwise as shown below, the results do not seem to indicate any ill effects of the initialization. The control experiment CON is the only experiment with no time-dependent forcing, thus any seen variations reflect the natural internal variability of the GS as it meanders and shed eddies. Five experiments test the impact of fluctuations of 100 ± 10 Sv in the GS outflow, but with different inflows. The impact of the FC is evaluated with three experiments, FC-02, FC-05, and FC-10, whereas the FC inflow from the south is forced by artificial fluctuations of 30 ± 10 Sv with periods of 2, 5, and 10 days, respectively, while holding the SC and SS inflows as constants at 40 and 30 Sv, respectively (see Table 1). Two other experiments, SC-05 and SS-05, evaluate the impact of ± 10 Sv fluctuations in the SC and SS inflows, while holding the other inflows at constant values. The last experiment, Wind-05, is set to evaluate the impact of the wind, introducing an artificial zonal wind fluctuations of $U = \pm 5$ m s⁻¹ with a 5-day period and no north/south component, $V = 0$. Experiments (not shown) comparing the simulations of the control run (constant monthly mean winds) with simulations with no wind at all, resulted in almost no visible effect on the CSL. The winds near the coast in the monthly mean data seem too weak (Fig. 3) to produce significant variations in CSL in this idealized smooth coast. On the

Fig. 4 Examples of Sea Surface Height (SSH in m; upper panels) and Sea Surface Temperature (SST in °C; lower panels) in the control run after 20 (left panels) and 40 (right panels) days following the spin-up

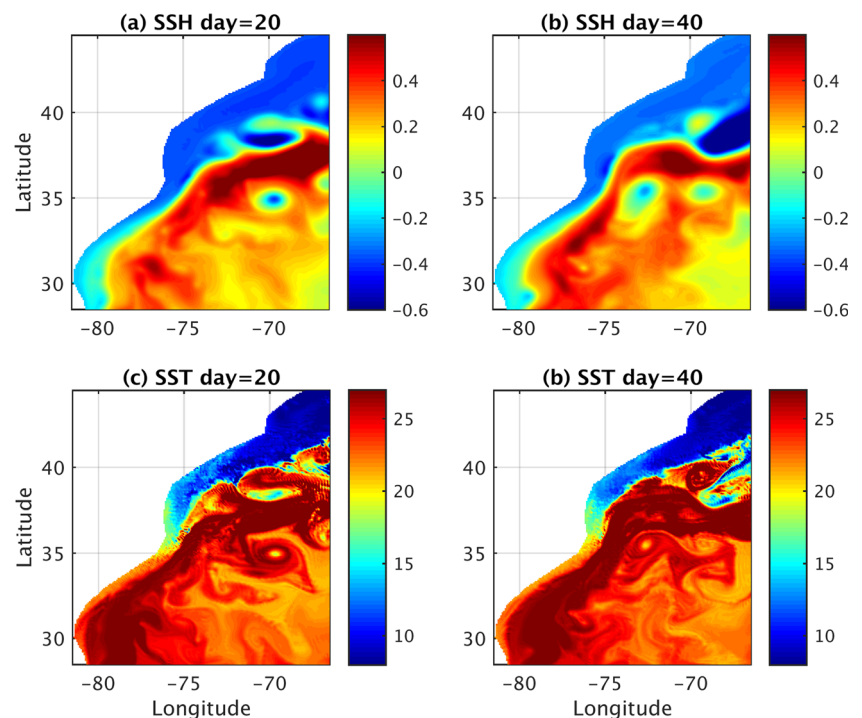


Table 1 Summary of model experiments. Inflow (+) and outflow (−) boundary conditions are specified for Florida Current (FC), Slope Current (SC), Sargasso Sea (SS), and Gulf Stream (GS); see Fig. 2b. The experiments with variable transports use sinusoidal function with the indicated amplitude and period relative to the constant transport of the control experiment

Experiment	Mean transports (Sv)				Period of oscillation	Wind
	FC	SC	SS	GS		
	+30	+40	+30	−100		
	Variations					
CON (control)	0	0	0	0	no oscillation	monthly mean
FC-02	±10	0	0	±10	2 days	monthly mean
FC-05	±10	0	0	±10	5 days	monthly mean
FC-10	±10	0	0	±10	10 days	monthly mean
SC-05	0	±10	0	±10	5 days	monthly mean
SS-05	0	0	±10	±10	5 days	monthly mean
Wind-05	0	0	0	0	5 days	$U = \pm 5$ m/s, $V = 0$

other hand, for the short-term variations that this study is focused on, the 5 m s^{-1} wind fluctuations with period of 5 days in experiments Wind-05 are quite typical onshore/offshore fluctuations seen in observations at this time of year. The aim here is to qualitatively compare wind-driven and GS-driven CSL variations. This comparison refers to local wind-driven sea level, since the impact of large-scale wind on the Atlantic circulation and the GS requires a basin-scale model and cannot be captured by the regional model.

3 Results

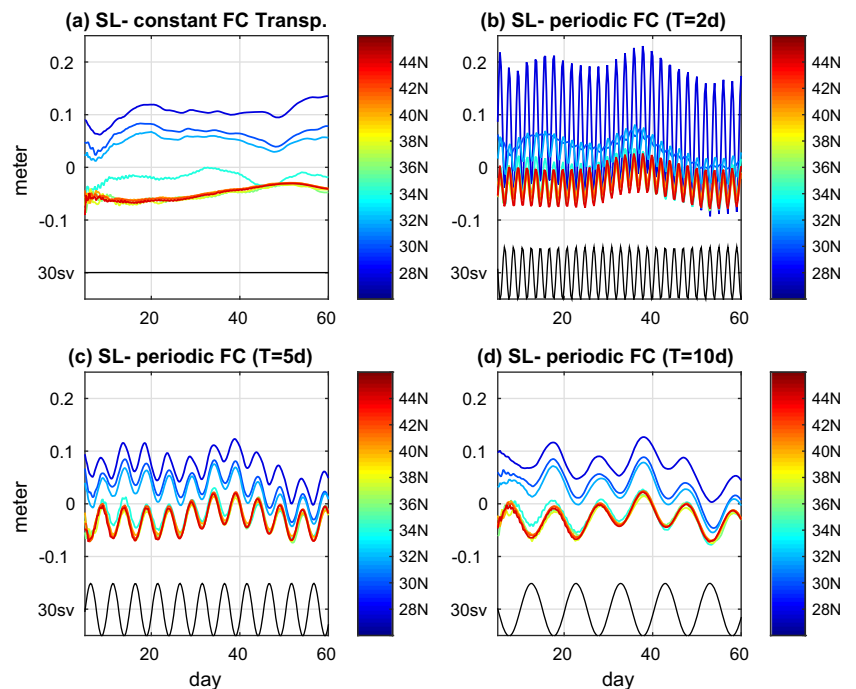
3.1 Impact of variations in the Florida Current transport

Figure 5 compares experiments FC-02, FC-05, and FC-10 (Fig. 5b–d) with the control run (Fig. 5a). Even in the control

case without any time-dependent forcing, there are temporal variations in CSL of ~5–10 cm within ~10–20 days time scales. Those variations, which can only be attributed to the natural fluctuations in the GS, are quite small, but non-negligible when compared with long-term SLR variations of say decadal changes or sea level rise rates of a few millimeters per year. There is a large spatial change in CSL of ~15 cm within the SAB (south of 36° N) when the GS flows close to shore, but little change in the northern half of the domain, in agreement with geoid models (see Fig. 1b in Higginson et al. 2015). Note also that the model results show some southward propagation of signals in the SAB (28° N – 34° N and days 45–50; Fig. 5a), in agreement with the expected propagation direction of CTW and the observations (Fig. 1).

When introducing high-frequency oscillations in the FC transport, CSL fluctuates at the same period as the forcing, but with opposite phase, so that CSL peaks when transport is

Fig. 5 Coastal sea level in the model every 2° N (blue to red lines are for locations 28° N to 44° N , respectively) for experiments with different period of FC transport oscillations: **a** Experiment CON, **b** Experiment FC-02, **c** Experiment FC-05, and **d** Experiment FC-10. The black line at the bottom of each panel represents the FC transport (see Table 1 for details)



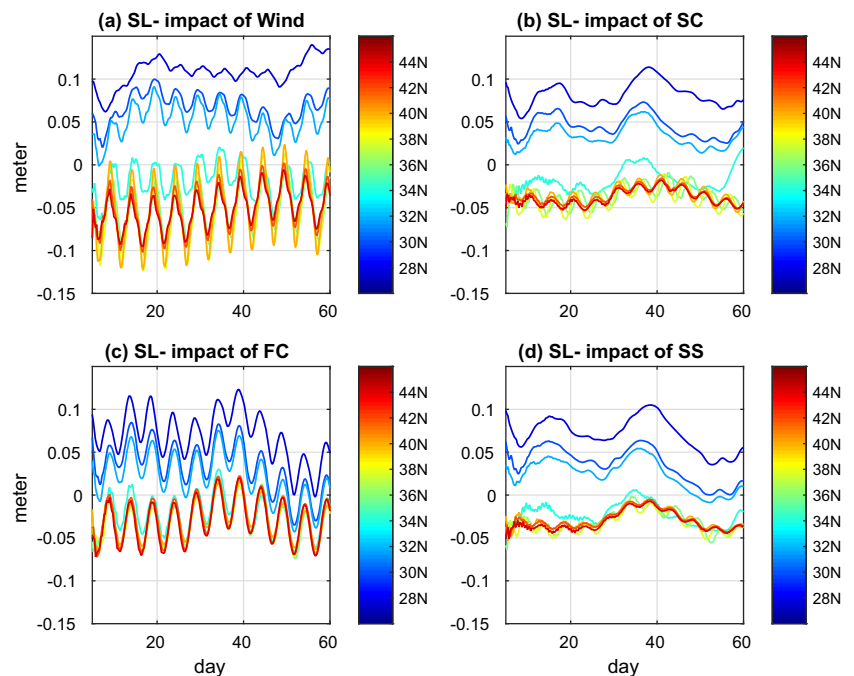
minimum, and the tilt of sea level across the GS is small (according to the geostrophic balance). These high-frequency oscillations are added to lower frequency fluctuations with ~ 20 -day period that are related to meso-scale natural variations in the GS. The largest amplitude of the oscillations is obtained in the SAB, close to the FC and when the frequency was highest (period $T=2$ days, Fig. 5b). Huthnance (2004) found the largest shelf sea level response when the frequency of the CTW was near resonance at $\omega=0.45f$ (f is the Coriolis parameter), i.e., when the period of the oscillations is around $T=2.22T_f$ (T_f is the inertial period). At 30°N $T_f=1$ day and $T(\text{resonance})\sim 2$ days, so for the case FC-02, a CTW resonance can be expected. This can explain why the amplification of the coastal response is maximum in the SAB and limited to an oscillating forcing with a 2-day period (Fig. 5b). Farther north in the MAB, a higher frequency forcing with a period of ~ 1.5 day will be needed to cause a resonance, so the amplitude of the CSL variations there is not a function of the frequency of the forcing (red lines in Fig. 5b–d). The variations of sea level along the coast are more coherent in the model than those seen in observations (Fig. 1), and the amplitudes in this idealized model with smooth topography are somewhat smaller than observed. The correlations between the FC transport and CSL in the model is in the range 0.6–0.9, which is somewhat larger than in observations; this is expected given the fact that in the model the GS variation is the only forcing, while in the observations, the GS may be responsible for only ~ 20 –40 % of the variability in CSL. The relative coherency of CSL variations along the coast (in both the model and observations) suggests that the signal is spread along the

coast through fast-moving barotropic shelf waves, possibly mode 0 Kelvin waves (Huthnance 2004) with an estimated propagation speed $C = \sqrt{gH}$, g is gravity and H is depth. Note that the forcing signal in the model is introduced in experiments FC simultaneously in the inflow at the southwestern corner of the model domain and in the outflow at the northeastern part of the domain (Table 1), which may explain why the CSL fluctuations in the model are more coherent than observations. It is also likely that fast-moving barotropic waves in the deep ocean spread the signal from the sources to the rest of the domain, before CTW are excited. The time it takes a disturbance to cross the entire model domain (~ 1500 km) is about 2.5 h if traveling in deep waters (say 3000 m) and about 20 h if traveling on the continental shelf (say average depth of ~ 50 m). In comparison, if a signal is traveling from the Florida Strait downstream with the GS current at a typical speed of ~ 1 m s $^{-1}$, it will take that signal ~ 17 days to reach the eastern boundary of the model, so the latter is clearly not the mechanism responsible for the coherent CSL variations seen here. Further analysis later will try to see if shelf waves can be detected in the model results.

3.2 Impact of Slope Current, Sargasso Sea flow and wind

Next, the impact of variations in the SC, SS, and wind are evaluated in Fig. 6. Experiments SC-05 and SS-05 (Fig. 6b, d, respectively) represent cases when the source of ± 10 Sv variations in the GS transport are fluctuations originated from the east; for example, changes in the sub-polar gyre that influence the SC or changes in the sub-tropical gyre that influence

Fig. 6 Same as Fig. 5, but for experiments with wind and different location of oscillating inflow: **a** Wind-05, **b** SC-05, **c** FC-05, and **d** SS-05. **c** Shows the same data as in Fig. 5c

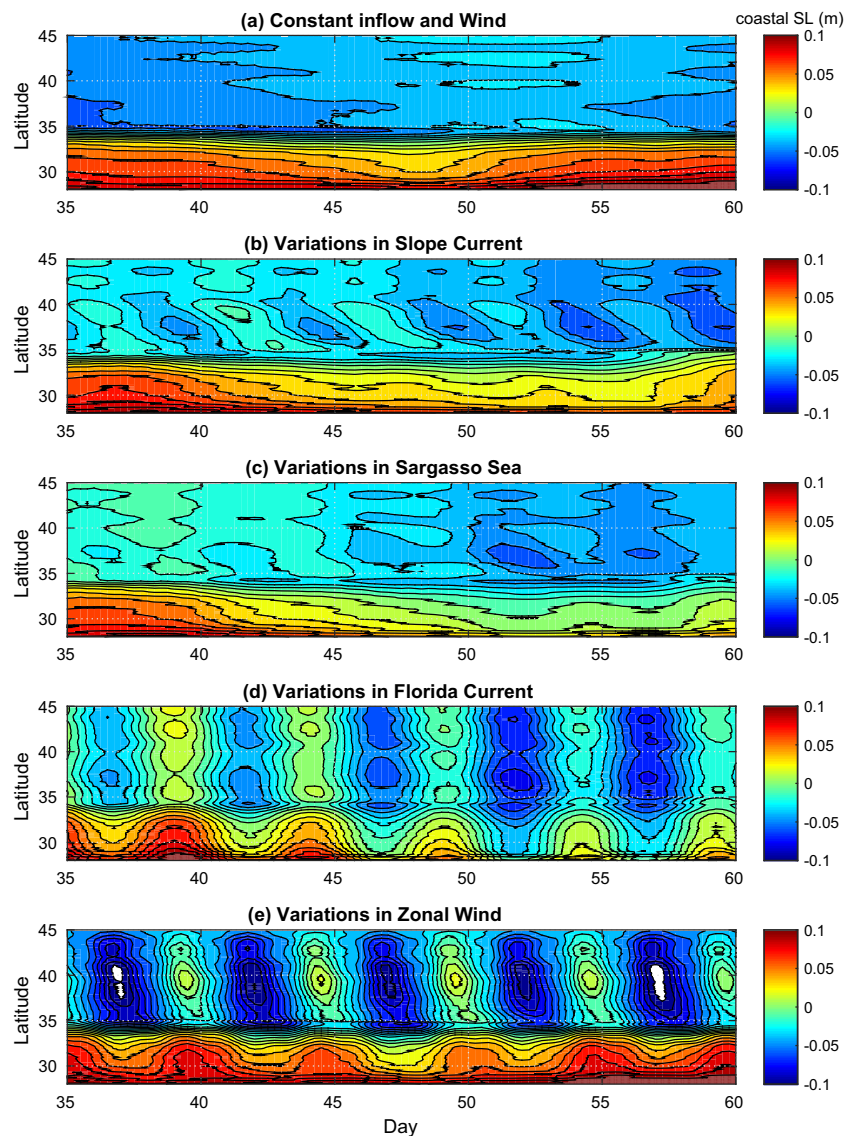


the SS. In those cases, the impact on the CSL is smaller than the impact of variations coming from the south (Fig. 6c; same as Fig. 5c), and the variations are limited to the coastal region north of Cape Hatteras; south of Cape Hatteras variations with a longer period are due to the meso-scale dynamics of the GS independent of the imposed variations. Cape Hatteras seems to block the propagation of the high-frequency signals coming from the north from moving south against the GS flow, but longer-term signals do seem to propagate southward (Fig. 6b, d). The southward propagation of signals along the coast can be seen even more clearly in Fig. 7. The various studies of CTW (Allen 1975; Wang and Mooers 1976; Huthnance 1978, 2004) indicate the large influence that the shelf and slope topography have on the characteristics of the waves, so it is not unexpected that the sudden change in topography at Cape Hatteras between the SAB in the south and the MAB in the north will limit communication between the shelf of the SAB

and that of the MAB, at least if information is transferred through along-coast CTW.

Experiment Wind-05, while not necessarily very realistic, sheds light on the differences between wind-driven CSL (Fig. 6a) and GS-driven CSL (Fig. 6c). First, note that the longer-term meso-scale driven variations are affected by the wind; for example, after day 40, CSL is rising in the wind-driven case but dropping in all the GS-driven cases. Second, though the amplitudes and coherency in phase of CSL variations generated by $\pm 5 \text{ m s}^{-1}$ zonal wind variations, are of the same order as those generated by $\pm 10 \text{ Sv}$ variations in the GS transport, there are significant differences between those cases. In the Wind-05 case, the amplitude of the CSL variations is increased northward where the continental shelf is wider than the narrow shelf in the SAB. This is expected from basic wind-driven coastal dynamics (Csanady 1982). The even amplitudes along the coast in the GS-driven case suggest

Fig. 7 Hovmöller diagram of sea level along the model's coast as a function of time and latitude for experiments: **a** CON, **b** SC-05, **c** SS-05, **d** FC-05, and **e** Wind-05

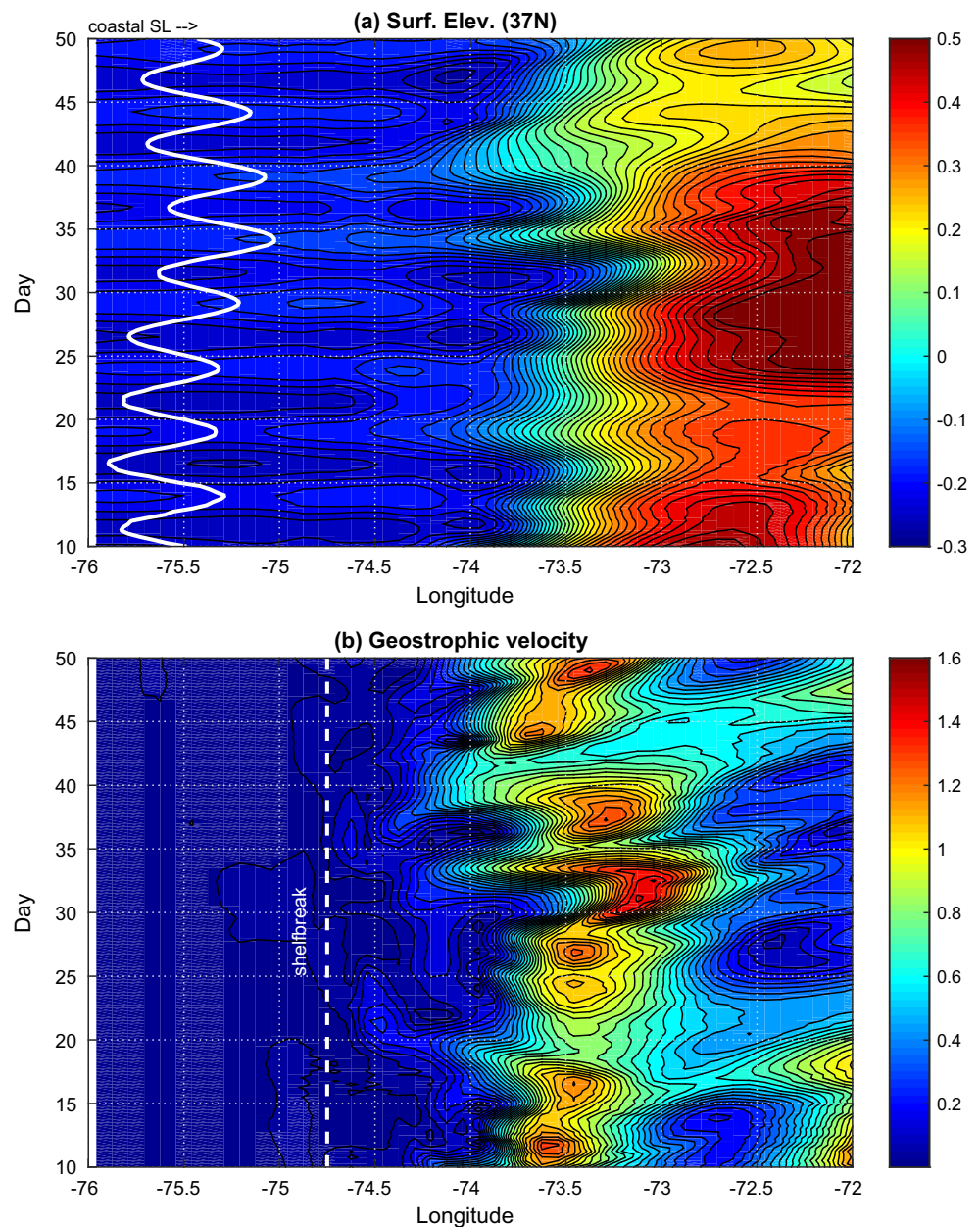


that the CSL is not driven by onshore/offshore transports on the shelf as in the wind-driven case, but rather is related to barotropic shelf waves.

To summarize the results, Fig. 7 compares the four experiments with cyclical forcing of 5-day oscillations with the control run using the so-called Hovmöller Diagram (CSL at the western coast versus time and latitude). In all the experiments, there is a barrier at $\sim 35^\circ$ N (near Cape Hatteras) between the behavior north and south of that latitude, which can be seen in the change in the propagation of signals across this latitude and the general lower/higher sea level north/south of this point. Past studies indicate differences between the regions north and south of Cape Hatteras, such as seen in the tilt of mean sea level (Higginson et al. 2015) and the spatial

pattern of change in sea level acceleration (Boon 2012; Sallenger et al. 2012; Ezer 2013; Boon and Mitchell 2015). This study shows that differences in the dynamics north and south of Cape Hatteras not only affect long-term variations, but also apply to high-frequency coastal variability. North of Cape Hatteras there are signs of southward propagation of waves along the western boundary; as expected from the theory of CTW, whereas all types of waves will tend to propagate southward along western boundaries of ocean basins in the northern hemisphere (Huthnance 1978). In the wind-driven case (Fig. 7e) and possibly in the FC-05 case (Fig. 7d), the signal propagates about 1000 km per day ($\sim 12 \text{ m s}^{-1}$), which is the speed that a barotropic Kelvin-like wave would propagate at water depth of ~ 15 m (close to the shallowest part of the

Fig. 8 Hovmöller diagram of **a** sea level (in m) in experiment FC-05 along 37° N as a function of longitude and time and **b** geostrophic velocity speed (in m s^{-1}) obtained from sea level gradients. Also shown in *white lines* are the coastal sea level (up is to the right with ~ 10 -cm range) and location of the shelfbreak (~ 100 -m depth)



model). Huthnance (2004) describes this type of barotropic adjustment that involves waves with group velocities of $\sim 10 \text{ m s}^{-1}$ and scales of $\sim 2000 \text{ km}$. On the other hand, when the imposed fluctuations are on the SC or SS, the signal seems to propagate much slower (Fig. 7b, c), at about 1000 km per week ($\sim 1.5 \text{ m s}^{-1}$), which indicates a type of baroclinic CTW. These slower-moving waves include baroclinic Kelvin waves, topographic shelf Rossby waves, and bottom trapped waves (or some combination of these waves) depending on the stratification and the shelf and slope shape (Wang and Mooers 1976). For the relatively flat shelf in the north part of the model domain, baroclinic Kelvin waves are more likely to be generated than the other types, and given the model stratification, their estimated propagation speed is $\sim 1 \text{ m s}^{-1}$.

To take a closer look at the connection between the deep ocean and the coast, Figs. 8 and 9 show the surface elevation and surface geostrophic velocity speed (calculated from surface elevation gradients) along 37° N (in the MAB, close to the GS sections studied in Ezer et al. 2013). In the FC-05

experiment, the imposed oscillations in the FC generate offshore/onshore meandering (Fig. 8a) and variations in the intensity (Fig. 8b) of the GS with a similar period (~ 5 days) to the forcing. There are coherent sea level variations on the continental shelf extending from the coast to $\sim 200 \text{ km}$ offshore (Fig. 8a), but there are no visible variations in velocity shoreward of the shelfbreak (Fig. 8b). In contrast, in the Wind-05 experiment, sea level variations on the shelf are limited to the near-coast region (no more than $\sim 50 \text{ km}$ from the coast; Fig. 9a), but the wind does generate visible velocity oscillations on the shelf with a period of 5 days (Fig. 9b).

The zonal wind also caused the GS to move closer to the shelfbreak at this latitude during this 40-day period. Note that intrusion of the GS into the shelfbreak has been identified long time ago in both, the SAB (Atkinson 1977) and the MAB (Bane et al. 1988). In this model experiment, this is an example of the influence of the GS path on CSL. When the GS moved $\sim 150 \text{ km}$ closer to the shore during ~ 30 -day period (Fig. 9), sea level along the coast rose by $\sim 3 \text{ cm}$ (white line in

Fig. 9 Same as Fig. 8, but for experiment Wind-05

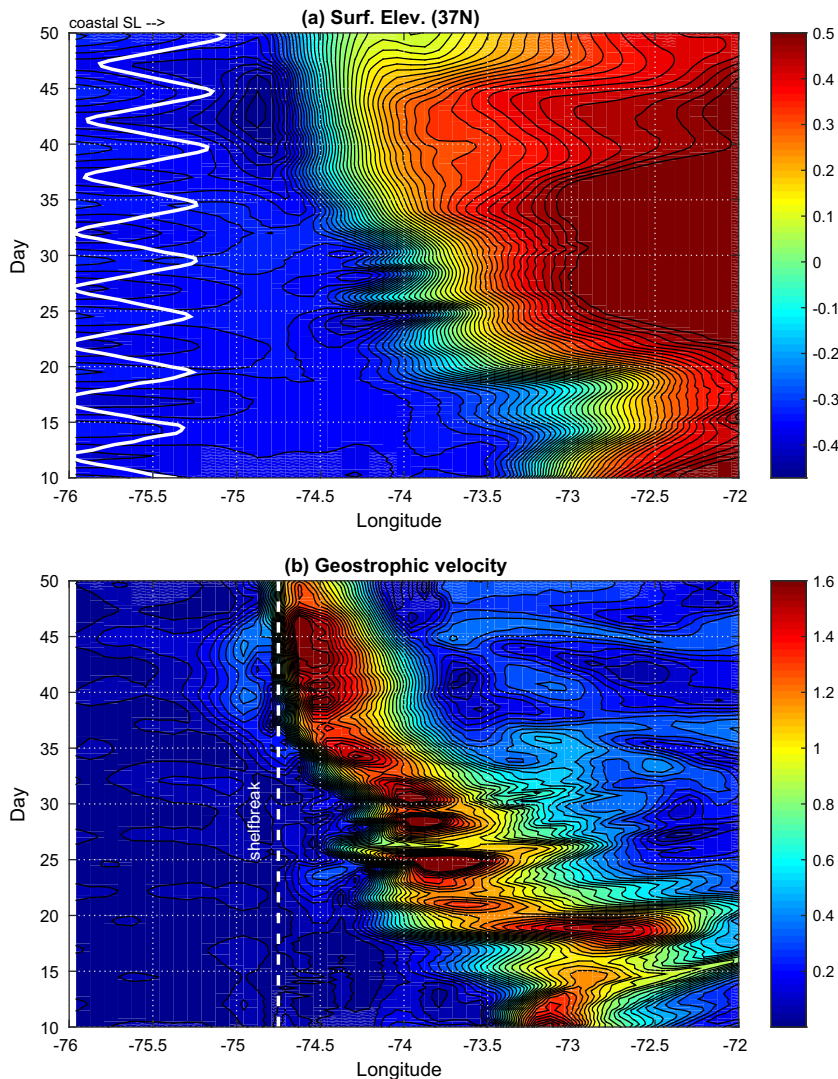


Fig. 9a). The temperature on the shelf did not change much, so this SLR does not seem to be due to steric effects. The SLR associated with the GS location is small, but it is ~ 100 times larger than the long-term SLR rate of $3\text{--}5\text{ mm year}^{-1}$ in the MAB (Boon 2012; Ezer 2013). The processes of high-frequency variations and CTW action addressed in the study may be quite different than longer-term variability of the GS and CSL; the latter processes need longer simulations and were addressed in other studies (e.g., Ezer 2015). However, the model results provide some hints of the impact of GS position that seem consistent with studies of long-term variations. For example, on interannual and decadal time scales, variations in NAO and AMOC and related changes in the GS transport were found to correlate with variations in the GS path (Ezer et al. 1995; Ezer 1999; Joyce et al. 2000; Joyce and Zhang 2010; Rossby et al. 2010) and apparently with variations in CSL (Ezer et al. 2013; Ezer 2015). On seasonal time scales, Xu and Oey (2011) also found similar results whereas CSL rises/falls when the GS moves onshore/offshore.

4 Summary and conclusions

There are many different drivers for variations in sea level along the coast that can impact a wide range of temporal scales, from daily variations in tides, winds, and air pressure, to decadal and multi-decadal climatic changes in atmospheric and oceanic circulation. One of the least understood process is how variations in CSL are related to changes in offshore currents, and in particular, how the GS impacts sea level along the US East Coast. Much attention has been given in recent years to potential connections between SLR and long-term climatic changes in AMOC and the GS (Levermann et al. 2005; Boon 2012; Ezer and Corlett 2012; Sallenger et al. 2012; Ezer 2013, 2015; Ezer et al. 2013; Kopp 2013; Yin and Goddard 2013; Srokosz and Bryden 2015). Less attention was given to short-term variations in the GS which may cause periods of days, weeks, or months with anomalously high water that increase the risk of tidal flooding (Sweet et al. 2009; Ezer and Atkinson 2014; Goddard et al. 2015) and beach erosion (Theuerkauf et al. 2014). Currently, water level prediction models are driven mostly by tides and local winds, so they may not be able to accurately simulate those remote, unpredictable and sometimes coherent anomalies as seen in Fig. 1.

This study is thus aimed at isolating the short-term GS-driven variations from other processes. This is achieved by using an idealized regional model of the GS and conducting sensitivity experiments with imposed variations in the GS transport, varying the frequency and location of the imposed oscillations. The regional model domain and boundary conditions are similar to the early model used by Mellor and Ezer (1991) and Ezer and Mellor (1992), but with a focus on the impact of the GS on short-term coastal variability. The

results show that an efficient way to induce coherent CSL variations along the US East Coast (similar to observations; Fig. 1) is by introducing oscillations in the transport of the FC. The variations in GS transport at the source first spread to the entire model domain through fast-moving deep-water barotropic waves, and then these large-scale signals generate CTW which result in coherent coastal sea level, in agreement with early studies of CTW (Allen 1975; Wang and Mooers 1976; Huthnance 1978). Because of the large sea level gradient across the GS, variations of few percentages in transport can be translated to non-negligible variations in sea level. Some discrepancies between the model results (Fig. 5) and observations (Fig. 1) can be explained by the way the idealized model was set up. For example, to maintain (almost exactly) volume conservation, the forced transport variations are simultaneously applied to the FC inflow and the GS outflow, resulting in a more coherent CSL signal than in observations; in observations variations in the GS transport are the result of changes in the wind, circulation, Rossby waves, etc., which can have spatial variability that is absent from this model. The process of transmission of large-scale open ocean signals into the shelf by CTW has been studied in details by Huthnance (2004) and can explain the finding of coherent CSL variations along many different coasts in the global ocean (Hughes and Meredith 2006). CTW can also explain the significant amplification of sea level variations on the SAB shelf seen in the model for one case (2-day oscillations; Fig. 5b)—in this case, the frequency of the forcing and the latitude have values near the CTW resonance predicted by Huthnance's study.

While short- and long-term processes may have different mechanisms of deep ocean-coast coupling, it is interesting to note the similarity between the results presented here and long-term GS-CSL connections. In both, long- and short-term forcing, weaker/stronger FC result in higher/lower CSL, consistent with the geostrophic balance. Because the model does not have any time-dependent forcing except the imposed inflow, the simulations prove that variations in the transport of the GS contribute to CSL variations. In addition, some unforced natural variations in the GS, as it meanders and shed eddies, also cause variations in CSL, but they are distinctively different than the imposed oscillations with the known cycle. In the real ocean, GS variations can originate from both, variations in the forcing (say wind) and unforced natural meso-scale variability, but both types can produce CSL variations, as shown here. While the idealized model demonstrates that the GS can cause coherent variations of CSL along the coast, the variations in observations have larger amplitude than the model variations since they include additional forcing that could also trigger coherent CSL.

An interesting result is the difference between GS variations induced by the inflow coming from the south (oscillations in the FC transport) and those coming from the east (SC or SS). In the latter cases, only the coastal region north of Cape

Hatteras was affected and was accompanied by what looks like southward moving baroclinic CTW. The smaller CSL variations induced by SC or SS variations may also be due to the fact that the disturbance in the SC and SS cases is more local, compared with the FC forcing cases that generate variations along the entire GS. Huthnance (2004) indicates that only the largest scales offshore anomalies may be able to generate CTW that can be detected at the coast. If one infers from the model results to processes in the real ocean, the simulations suggest that the impact on coastal variations from dynamic changes in the Sub-tropical Gyre (e.g., Zhao and Johns 2014) may be different than changes originated in the Sub-polar Gyre (e.g., Hakkinen and Rhines 2004) that affect the southward flowing SC (Rossby et al. 2010). All the experiments show distinct differences in the coastal dynamics north and south of the separation point of the GS at Cape Hatteras. CTW are largely affected by the shelf and slope topography, and the topography dramatically changes at Cape Hatteras which separates between the SAB and the MAB. Interestingly enough, other dynamic processes also change between the SAB and the MAB, such as the tilt of mean sea level along the coast (Higginson et al. 2015) and the distinct pattern of SLR acceleration with higher/lower acceleration in the MAB/SAB (Sallenger et al. 2012; Boon 2012; Ezer 2013). Therefore, it seems that Cape Hatteras provides a separation point for both, short- and long-term processes.

Although the short idealized simulations are process-oriented and do not intend to produce the most realistic results, they gave an opportunity to compare the GS-driven CSL variability with a more well-recognized, wind-driven CSL variability. In this simplified model, CSL variations of ~ 10 cm were generated by either ~ 10 Sv variations in the GS transport or ~ 5 m s⁻¹ variations in zonal wind. While the CSL variations look similar in the two cases, the mechanisms were very different, one involves barotropic CTW (GS-driven case) and one involves pile up of water due to onshore transport (wind-driven case).

The study demonstrates the usefulness of an idealized model to study basic dynamic processes, thus this model will be used for further studies of the role of various forcing and topography in GS dynamics, in follow-up experiments now underway. There could also be some practical implications for this study in improving operational coastal forecast systems of the US East Coast (Aikman et al. 1996) and providing better warning for flood risks in low-lying coastal areas (Ezer and Atkinson 2014).

Acknowledgments Old Dominion University's Climate Change and Sea Level Rise Initiative (CCSLRI) provided partial support for this study. The hourly tide gauges sea level data are available from: <http://tidesandcurrents.noaa.gov/>. The monthly reanalysis of temperature and

salinity (ARMOR3D) and wind data (ASCAT) were obtained from MyOcean-Copernicus site: <http://marine.copernicus.eu/>. The Florida Current transport data is obtained from: <http://www.aoml.noaa.gov/phod/floridacurrent/>. Reviewers provided useful suggestions that helped to improve the manuscript.

References

- Aikman F, Mellor GL, Ezer T, Shenin D, Chen P, Breaker L, Rao DB (1996) Toward an operational nowcast/forecast system for the U.S. East Coast, In: Modern approaches to data assimilation in ocean modeling. Malanotte-Rizzoli P (ed). Elsevier Oceanog Ser 61:347–376. doi:10.1016/S0422-9894(96)80016-X
- Allen JS (1975) Coastal trapped waves in a stratified ocean. *J Phys Oceanogr* 5:300–325
- Atkinson LP (1977) Modes of Gulf Stream intrusion into the South Atlantic Bight shelf waters. *Geophys Res Lett* 4(12):583–586
- Bane JM, Brown OB, Evans RH, Hamilton P (1988) Gulf Stream remote forcing of shelfbreak currents in the Mid-Atlantic Bight. *Geophys Res Lett* 15(5):405–407
- Baringer MO, Larsen JC (2001) Sixteen years of Florida current transport at 27N. *Geophys Res Lett* 28(16):3,179–3,182
- Bentamy A, Fillon DC (2012) Gridded surface wind fields from Metop/ASCAT measurements. *Int J Remote Sens* 33(6):1729–1754
- Blaaha JP (1984) Fluctuations of monthly sea level as related to the intensity of the Gulf Stream from Key West to Norfolk. *J Geophys Res Oceans* 89(C5):8033–8042
- Boon JD (2012) Evidence of sea level acceleration at U.S. and Canadian tide stations, Atlantic coast, North America. *J Coast Res* 28(6): 1437–1445. doi:10.2112/JCOASTRES-D-12-00102.1
- Boon JD, Mitchell M (2015) Nonlinear change in sea level observed at North American tide stations. *J Coast Res.* 31(6):1295–1305. doi:10.2112/JCOASTRES-D-15-00041.1
- Bryden HL, Longworth HR, Cunningham SA (2005) Slowing of the Atlantic meridional overturning circulation at 25°N. *Nature* 438. doi:10.1038/nature04385
- Csanady GT (1982) Circulation in the coastal ocean. Reidel, Dordrecht, 279 pp
- Ezer T (1999) Decadal variabilities of the upper layers of the subtropical North Atlantic: an ocean model study. *J Phys Oceanogr* 29(12): 3111–3124. doi:10.1175/1520-0485(1999)029
- Ezer T (2001) Can long-term variability in the Gulf Stream transport be inferred from sea level? *Geophys Res Lett* 28(6):1031–1034. doi:10.1029/2000GL011640
- Ezer T (2006) Topographic influence on overflow dynamics: idealized numerical simulations and the Faroe Bank Channel overflow. *J Geophys Res* 111(C02002). doi:10.1029/2005JC003195
- Ezer T (2013) Sea level rise, spatially uneven and temporally unsteady: why the U.S. East Coast, the global tide gauge record, and the global altimeter data show different trends. *Geophys Res Lett* 40:5439–5444. doi:10.1002/2013GL057952
- Ezer T (2015) Detecting changes in the transport of the Gulf Stream and the Atlantic overturning circulation from coastal sea level data: the extreme decline in 2009–2010 and estimated variations for 1935–2012. *Glob Planet Chang* 129:23–36. doi:10.1016/j.gloplacha.2015.03.002
- Ezer T, Atkinson LP (2014) Accelerated flooding along the U.S. East Coast: on the impact of sea-level rise, tides, storms, the Gulf Stream, and the North Atlantic Oscillations. *Earth's Future* 2(8): 362–382. doi:10.1002/2014EF000252
- Ezer T, Corlett WB (2012) Is sea level rise accelerating in the Chesapeake Bay? A demonstration of a novel new approach for analyzing sea

- level data. *Geophys Res Lett* 39(L19605). doi:[10.1029/2012GL053435](https://doi.org/10.1029/2012GL053435)
- Ezer T, Mellor GL (1992) A numerical study of the variability and the separation of the Gulf Stream, induced by surface atmospheric forcing and lateral boundary flows. *J Phys Oceanogr* 22:660–682
- Ezer T, Mellor GL (1994) Diagnostic and prognostic calculations of the North Atlantic circulation and sea level using a sigma coordinate ocean model. *J Geophys Res* 99(C7):14,159–14,171. doi:[10.1029/94JC00859](https://doi.org/10.1029/94JC00859)
- Ezer T, Mellor GL, Greatbatch RJ (1995) On the interpentadal variability of the North Atlantic Ocean: model simulated changes in transport, meridional heat flux and coastal sea level between 1955–1959 and 1970–1974. *J Geophys Res* 100(C6):10,559–10,566. doi:[10.1029/95JC00659](https://doi.org/10.1029/95JC00659)
- Ezer T, Atkinson LP, Corlett WB, Blanco JL (2013) Gulf Stream's induced sea level rise and variability along the U.S. mid-Atlantic coast. *J Geophys Res* 118:685–697. doi:[10.1002/jgrc.20091](https://doi.org/10.1002/jgrc.20091)
- Ferry N, Parent L, Garric G, Barnier B, Molines J-M, Guinehut S, Mulet S, Haines K, Valdivieso M, Masina S, Storto A (2012) MYOCEAN eddy-permitting global ocean reanalysis products: description and results. Proc. 20 Years of Progress in Radar Altimetry Symposium 24–29 September, Venice, Italy
- Goddard PB, Yin J, Griffies SM, Zhang S (2015) An extreme event of sea-level rise along the Northeast coast of North America in 2009–2010. *Nature Comm* 6. doi:[10.1038/ncomms7346](https://doi.org/10.1038/ncomms7346)
- Hakkinen S, Rhines PB (2004) Decline of subpolar North Atlantic circulation during the 1990s. *Science* 304:555–559. doi:[10.1126/science.1094917](https://doi.org/10.1126/science.1094917)
- Higginson S, Thompson KR, Woodworth PL, Hughes CW (2015) The tilt of mean sea level along the east coast of North America. *Geophys Res Lett* 42(5):1471–1479. doi:[10.1002/2015GL063186](https://doi.org/10.1002/2015GL063186)
- Hogg NG (1992) On the transport of the Gulf Stream between cape Hatteras and the grand banks. *Deep-Sea Res* 39(7–8):1231–1246. doi:[10.1016/0198-0149\(92\)90066-3](https://doi.org/10.1016/0198-0149(92)90066-3)
- Hughes CW, Meredith PM (2006) Coherent sea-level fluctuations along the global continental slope. *Philos Trans R Soc* 364:885–901. doi:[10.1098/rsta.2006.1744](https://doi.org/10.1098/rsta.2006.1744)
- Huthnance JM (1978) On coastal trapped waves: analysis and numerical calculation by inverse iteration. *J Phys Oceanogr* 8:74–92
- Huthnance JM (2004) Ocean-to-shelf signal transmission: a parameter study. *J Geophys Res* 109(C12029). doi:[10.1029/2004JC002358](https://doi.org/10.1029/2004JC002358)
- Joyce TM, Zhang R (2010) On the path of the Gulf Stream and the Atlantic meridional overturning circulation. *J Clim* 23:3146–3154. doi:[10.1175/2010JCLI3310.1](https://doi.org/10.1175/2010JCLI3310.1)
- Joyce TM, Deser C, Spall MA (2000) The relation between decadal variability of subtropical mode water and the North Atlantic oscillation. *J Clim* 13:2550–2569. doi:[10.1175/1520-0442\(2000\)013](https://doi.org/10.1175/1520-0442(2000)013)
- Kopp RE (2013) Does the mid-Atlantic United States sea-level acceleration hot spot reflect ocean dynamic variability? *Geophys Res Lett* 40(15):3981–3985. doi:[10.1002/grl.50781](https://doi.org/10.1002/grl.50781)
- Levermann A, Griesel A, Hofmann M, Montoya M, Rahmstorf S (2005) Dynamic sea level changes following changes in the thermohaline circulation. *Clim Dyn* 24(4):347–354
- McCarthy G, Frejka-Williams E, Johns WE, Baringer MO, Meinen CS, Bryden HL, Rayner D, Duchez A, Roberts C, Cunningham SA (2012) Observed interannual variability of the Atlantic meridional overturning circulation at 26.5°N. *Geophys Res Lett* 39(19). doi:[10.1029/2012GL052933](https://doi.org/10.1029/2012GL052933)
- Mellor GL, Ezer T (1991) A Gulf Stream model and an altimetry assimilation scheme. *J Geophys Res* 96:8779–8795. doi:[10.1029/91JC00383](https://doi.org/10.1029/91JC00383)
- Mellor GL, Mechoso CR, Keto E (1982) A diagnostic calculation of the general circulation of the Atlantic Ocean. *Deep Sea Res* 29(10):1171–1192
- Mellor GL, Hakkinen S, Ezer T, Patchen R (2002) A generalization of a sigma coordinate ocean model and an intercomparison of model vertical grids. In: *Ocean forecasting: conceptual basis and applications*. Pinardi N, Woods ED (Eds). Springer 55–72. doi:[10.1007/978-3-662-22648-3_4](https://doi.org/10.1007/978-3-662-22648-3_4)
- Montgomery R (1938) Fluctuations in monthly sea level on eastern U.S. Coast as related to dynamics of western North Atlantic Ocean. *J Mar Res* 1:165–185
- Piecuch CG, Ponte RM (2015) Inverted barometer contributions to recent sea level changes along the northeast coast of North America. *Geophys Res Lett* 42(14). doi:[10.1002/2015GL064580](https://doi.org/10.1002/2015GL064580)
- Rossby T, Flagg C, Donohue K (2010) On the variability of Gulf Stream transport from seasonal to decadal timescales. *J Mar Res* 68:503–522
- Rossby T, Flagg CN, Donohue K, Sanchez-Franks A, Lillibridge J (2014) On the long-term stability of Gulf Stream transport based on 20 years of direct measurements. *Geophys Res Lett* 41:114–120. doi:[10.1002/2013GL058636](https://doi.org/10.1002/2013GL058636)
- Sallenger AH, Doran KS, Howd P (2012) Hotspot of accelerated sea-level rise on the Atlantic coast of North America. *Nat Clim Chang* 2:884–888. doi:[10.1038/NCILMATE1597](https://doi.org/10.1038/NCILMATE1597)
- Smeed DA, McCarthy G, Cunningham SA, Frajka-Williams E, Rayner D, Johns WE, Meinen CS, Baringer MO, Moat BI, Duchez A, Bryden HL (2013) Observed decline of the Atlantic meridional overturning circulation 2004 to 2012. *Ocean Sci Discuss* 10:1619–1645. doi:[10.5194/osd-10-1619-2013](https://doi.org/10.5194/osd-10-1619-2013)
- Srokosz MA, Bryden HL (2015) Observing the Atlantic meridional overturning circulation yields a decade of inevitable surprises. *Science* 348(6241):1255575. doi:[10.1126/science.1255575](https://doi.org/10.1126/science.1255575)
- Sturges W (1974) Sea level slope along continental boundaries. *J Geophys Res* 79(6):825–830
- Sturges WB, Hong G (2001) Gulf Stream transport variability at periods of decades. *J Phys Oceanogr* 31:1304–1312
- Sweet W, Park J (2014) From the extreme to the mean: acceleration and tipping points of coastal inundation from sea level rise. *Earth's Future* 2(12):579–600
- Sweet W, Zervas C, Gill S (2009) Elevated east coast sea level anomaly: June–July 2009. NOAA Tech Rep No NOS CO-OPS 051, 40 pp., NOAA Natl. Ocean Service, Silver Spring, Md
- Theuerkauf EJ, Rodriguez AB, Fegley SR, Luettich RA (2014) Sea level anomalies exacerbate beach erosion. *Geophys Res Lett* 41(14):5139–5147. doi:[10.1002/2014GL060544](https://doi.org/10.1002/2014GL060544)
- Thompson PR, Mitchum GT (2014) Coherent sea level variability on the North Atlantic western boundary. *J Geophys Res Oceans* 119:5676–5689. doi:[10.1002/2014JC009999](https://doi.org/10.1002/2014JC009999)
- Wang D-P, Mooers CNK (1976) Coastal-trapped waves in a continuously stratified ocean. *J Phys Oceanogr* 6:853–863. doi:[10.1175/1520-0485\(1976\)006<0853:CTWIAC>2.0.CO;2](https://doi.org/10.1175/1520-0485(1976)006<0853:CTWIAC>2.0.CO;2)
- Woodworth PL, Maqueda M, Roussenov MÁ, Williams VM, Hughes RG (2014) Mean sea level variability along the northeast American Atlantic coast, and the roles of the wind and the overturning circulation. *J Geophys Res Oceans* 119(12):8916–8935. doi:[10.1002/2014JC010520](https://doi.org/10.1002/2014JC010520)
- Xu F-H, Oey L-Y (2011) The origin of along-shelf pressure gradient in the Middle Atlantic Bight. *J Phys Oceanogr* 41(9):1720–1740. doi:[10.1175/2011JPO4589](https://doi.org/10.1175/2011JPO4589)
- Yin J, Goddard PB (2013) Oceanic control of sea level rise patterns along the East Coast of the United States. *Geophys Res Lett* 40:5514–5520. doi:[10.1002/2013GL057992](https://doi.org/10.1002/2013GL057992)
- Zhao J, Johns W (2014) Wind-forced interannual variability of the Atlantic meridional overturning circulation at 26.5°N. *J Geophys Res Oceans* 119:6253–6273. doi:[10.1002/2013JC009407](https://doi.org/10.1002/2013JC009407)